npj | parkinson's disease

Article

Published in partnership with the Parkinson's Foundation

https://doi.org/10.1038/s41531-025-00985-2

Investigating glymphatic function and bed nucleus of the stria terminalis-based functional connectivity in Parkinson's disease with and without depression

Xiyong Dai[1,2,5], Yue Zhang[2,5], Chengwei Fu[1,2], Zhijie Gao[1,2], Xiaoyan Hou[2], Zhaoxian Yan[2], Chunye Zheng[3], Lei Gao[4] & Bo Liu[2]

Glymphatic activity and the bed nucleus of the stria terminalis (BNST) have been implicated in the pathogenesis of Parkinson's disease (PD) with depression (PDD). This study aimed to investigate glymphatic function and BNST-based functional connectivity (FC) and potential biomarkers in PDD. The diffusion tensor imaging analysis along the perivascular space (DTI-ALPS) index combined with BNST-based FC and support vector machine were applied to 24 PDD, 24 PD with non-depression (PDND), and 25 healthy controls. We found that (1) the DTI-ALPS indices ($p < 0.001$), the right BNST-based FC values ($p < 0.001$, FWE small volume correction) were significantly different among three groups; (2) the FC features in the right mPFC (mPFC_R), right MTG (MTG_R), and right ITG (ITG_R) can distinguish PDD from PDND; (3) the right BNST-based FC values, DTI-ALPS indices, and HAMD scores were correlated with each other ($r = -0.620$, $p = 0.004$; $r = 0.651$, $p = 0.002$; $r = -0.53$, $p = 0.016$). Impaired glymphatic function and altered BNST-based FC values are strongly associated with PD, and brain regions with differences in the right BNST-based FC values may serve as potential biomarkers for classifying clinical subtypes of PD. These findings provide new insights into the pathogenesis of depression in PD. This study protocol was registered on the Chinese Clinical Trial Registry (ChiCTR2000038411, September 22, 2020, https://www.chictr.org.cn/showproj.html?proj=56715).

Parkinson's disease (PD) is the second most common neurodegenerative disorder, affecting approximately 6.1 million people worldwide in 2016, and is a major public health issue and global priority[1–3]. Pathologically, PD is characterized by the accumulation, deposition, and impaired clearance of α-synuclein in Lewy bodies and Lewy neurites[4–6]. More importantly, glymphatic system is the brain's waste removal pathway and involves fluid exchange between interstitial space and perivascular space (PVS)[7]. Therefore, investigating the glymphatic system may help to uncover the pathophysiological mechanisms of PD.

Currently, most studies of the glymphatic system are based on animal models, and their methods are invasive[8–10]. In 2017, Taoka et al. first used an approach based on diffusion tensor imaging analysis along the perivascular space (DTI-ALPS) to study the glymphatic system in humans. This method is a non-invasive, convenient, and promising indicator of glymphatic function in the brain, which has been recognized by researchers and widely used in a variety of diseases[11–16]. Thus, the DTI-ALPS approach provides an opportunity to non-invasively investigate the glymphatic system in PD.

Of note, the prevalence of PD-related depression in PD varies widely between different studies, ranging from 2.7% to 90%, and it accelerates the progression of disease and reduces the quality of life in PD[17–19]. However, due to the lack of sufficient attention to depression and its severity in PD, most patients do not receive timely and appropriate treatment. The bed nucleus of the stria terminalis (BNST), located in the basal forebrain, is part

[1]The Second Clinical College of Guangzhou University of Chinese Medicine, Guangzhou, China. [2]Department of Radiology, The Second Affiliated Hospital of Guangzhou University of Chinese Medicine, Guangzhou, China. [3]Department of Neurology, The Second Affiliated Hospital of Guangzhou University of Chinese Medicine, Guangzhou, China. [4]Department of Radiology, Zhongnan Hospital of Wuhan University, Hubei, China. [5]These authors contributed equally: Xiyong Dai, Yue Zhang. e-mail: liubogzcm@163.com

of the extended amygdala[20,21]. The BNST has extensive afferent and efferent connections, and its main functions are related to negative emotions and stress (i.e., anxiety)[22,23]. The link between the BNST and depression has been confirmed by studies in which both BNST-targeted deep brain stimulation and injection of adrenergic receptor antagonists into the BNST can alleviate depression[24–27]. However, the role of the BNST in PD-related depression remains unclear.

Clinically, the diagnosis of affective symptoms in PD (i.e., depression, anxiety) relies on the subjective assessment of patients' complaints and symptoms by clinicians, and objective neuroimaging biomarkers are lacking. Therefore, the search for objective and reliable neuroimaging biomarkers will aid not only in the diagnostic decisions but also in the classification and management of PD.

In this paper, to address the above issues, we applied DTI-ALPS to detect the alterations in the glymphatic system, the seed-based functional connectivity (FC) to investigate the changes between the right BNST and the whole brain, a support vector machine (SVM) with the seed-based FC values of the differential brain regions to identify the optimal brain regions that can discriminate PDD from PDND.

Results

Demographics and clinical scales assessment

In total, 48 PD with or without depression and 25 HC were recruited. Table 1 reveals detailed demographic and clinical characteristics of all participants. HC and PDD, PDND were matched for age and gender. There were no significant differences between three groups in gender, age, education, and Mini-Mental State Examination (MMSE) scores, but there were significant differences in HAMA, HAMD, BDI, and MADRS ($p < 0.05$).

However, individuals with PDD had significantly higher UPDRS scores and H&Y stage ($p = 0.026$) than those with PDND, including UPDRS total scores ($p = 0.003$), UPDRS I ($p < 0.001$), UPDRS II ($p = 0.004$), and UPDRS III ($p = 0.014$).

Table 1 | Demographic characteristics and clinical measurements of the included participants

Variables	Patients		HC (n = 25)	*F/Z* value	*P* value
	PDD (n = 24)	PDND (n = 24)			
Age	66.46 ± 8.19	64.50 ± 9.93	62.28 ± 6.88	3.24	0.198[a]
Education	11.71 ± 3.44	13.42 ± 2.64	12.32 ± 2.82	3.31	0.190[a]
Gender (M/F)	14/10	11/13	11/14	1.18	0.554[b]
HAMA*	10.71 ± 3.99	6.58 ± 3.22	3.00 ± 4.04	34.74	0.000[a]
HAMD*	16.08 ± 5.33	4.92 ± 1.91	4.04 ± 1.97	44.98	0.000[a]
MADRS*	12.46 ± 5.90	4.88 ± 3.27	2.84 ± 4.29	37.78	0.000[a]
BDI*	8.63 ± 3.44	3.58 ± 2.19	2.32 ± 3.42	37.29	0.000[a]
UPDRS total*	70.79 ± 26.83	47.71 ± 21.04	NA	−3.02	0.003[c]
UPDRS I*	11.08 ± 3.84	6.67 ± 3.14	NA	−3.62	0.000[c]
UPDRS II*	13.88 ± 6.26	8.71 ± 5.81	NA	−2.89	0.004[c]
UPDRS III*	42.92 ± 17.92	30.92 ± 13.53	NA	−2.47	0.014[c]
UPDRS IV	2.92 ± 3.79	1.42 ± 2.30	NA	−1.00	0.316[c]
H&Y stage*	2.33 ± 0.67	1.89 ± 0.64	NA	−2.23	0.026[c]
MMSE	28.38 ± 1.81	28.88 ± 1.23	28.24 ± 1.39	2.38	0.305[a]

M male, *F* female, *HAMA* Hamilton Anxiety Scale, *HAMD* Hamilton Depression Scale, *MADRS* Montgomery-Asberg Depression Rating Scale, *BDI* Beck's Depression Inventory, *UPDRS* unified Parkinson's disease rating scale, *H&Y* stage Hoehn & Yahr stage, *NA* not applicable, *PD* Parkinson's disease, *PDD* PD patients with depression, *PDND* PD patients with non-depression, *HC* healthy control, *MMSE* Mini-Mental State Examination.
[a]*p* values were obtained by Kruskal–Wallis test.
[b]*p* value for the gender difference was obtained by chi-square test.
[c]*p* values were obtained by Mann–Whitney U test.

Differences between groups in DTI-ALPS indices

The intraclass correlation coefficient (ICC) for the DTI-ALPS index between two raters was 0.82, indicating excellent reliability.

Significant differences were found in the right, left, and average DTI-ALPS indices between PDD, PDND, and HC ($p < 0.001$) (Table 2 and Fig. 1). Post hoc tests showed that the right, left, and average DTI-ALPS indices in PDD (1.180 ± 0.078; 1.141 ± 0.081; 1.160 ± 0.065) were significantly lower than those in PDND (1.276 ± 0.144; 1.254 ± 0.115; 1.265 ± 0.122), and the right, left, and average ALPS indices in PDND were significantly lower than those in HC (1.386 ± 0.106; 1.361 ± 0.137; 1.373 ± 0.107) ($p < 0.05$).

Differences between groups in seed-based functional connectivity

We selected the right BNST as the ROI, and then performed FC analysis using a seed-based approach to obtain FC values by calculating the Pearson's correlation coefficients between the ROI and the rest of the whole brain. The statistical results revealed that there were significant statistical differences ($p < 0.001$, FWE small volume correction) in the FC values of the BNST-mPFC_R, BNST-MTG_R and BNST-ITG_R between three groups (Table 3 and Fig. 2). Post-hoc tests showed that the seed-based FC values of the BNST-mPFC_R (0.149 ± 0.122), BNST-MTG_R (0.129 ± 0.110) and BNST-ITG_R (0.132 ± 0.144) in PDND were significantly higher than those in PDD, while the seed-based FC values of the BNST-mPFC_R (0.043 ± 0.082) and BNST-MTG_R (0.034 ± 0.113) in PDD were higher than those in HC ($p < 0.05$).

SVM-based classification

Using the seed-based FC values of the between-group differences as input variables (Table 4 and Fig. 3A), including ITG_R, MTG_R, and mPFC_R, a linear support vector machine was used to build a classifier. Accuracy varied with the number of features (Fig. 3B). We found that the top 70 meaningful features significantly contributed to the classifier's ability to discriminate PDD from PDND with high accuracy (accuracy = 85.4167, sensitivity = 87.5000, specificity = 83.3333, AUC = 0.8472) (Fig. 3D). Performing 5000 permutation tests on the classification results showed that our classifier had a good performance and was better than the random classifier ($p = 0.0006$) (Fig. 3C).

Correlation of DTI-ALPS and seed-based functional connectivity with clinical scales

Figure 4 revealed the associations between the DTI-ALPS indices, seed-based FC values, and HAMD scores in PDD. Notably, the seed-based FC values in the right ITG were positively correlated with the HAMD scores ($r = 0.651$, $p = 0.002$) (Fig. 4B), while the left DTI-ALPS indices were negatively correlated with the HAMD scores ($r = -0.53$, $p = 0.016$) (Fig. 4A) and the seed-based FC values in the mPFC_R ($r = -0.620$, $p = 0.004$) (Fig. 4C). However, we did not find any correlation between the DTI-ALPS indices, HAMA and MMSE scores in PDD.

Discussion

In this study, we investigated the differences in DTI-ALPS index between PDD, PDND, and HC groups. Then, we selected the right BNST as the ROI and performed FC analysis using a seed-based approach to obtain FC values between the ROI and the rest of the whole brain. Finally, we used a SVM with the seed-based FC values of the differential brain regions as input variables to identify the optimal brain regions that can discriminate PDD from PDND. The findings were as follows: (1) the left, right, and average DTI-ALPS indices were significantly different among three groups, with the right, left, and average DTI-ALPS indices being significantly lower in PDD than in PDND, and the left, right, and average DTI-ALPS indices being significantly lower in PDND than in HC; (2) the FC values of the

Table 2 | Between-group differences in DTI-ALPS index between PDD, PDND, and HC groups

Variables	Patients		HC	*F* value	*P* value	Multiple comparisons
	PDD	PDND				
ALPS_L	1.180 ± 0.078	1.276 ± 0.144	1.386 ± 0.106	20.629	0.000[a]	PDD < PDND PDD < HC HC > PDND
ALPS_R	1.141 ± 0.081	1.254 ± 0.115	1.361 ± 0.137	22.901	0.000[a]	PDD < PDND PDD < HC HC > PDND
ALPS_average	1.160 ± 0.065	1.265 ± 0.122	1.373 ± 0.107	27.147	0.000[a]	PDD < PDND PDD < HC HC > PDND

ALPS analysis along the perivascular space, *PD* Parkinson's disease, *PDD* PD patients with depression, *PDND* PD patients with non-depression, *HC* healthy control, *L* left, *R* right.
[a]*p* values were obtained by Kruskal–Wallis test.

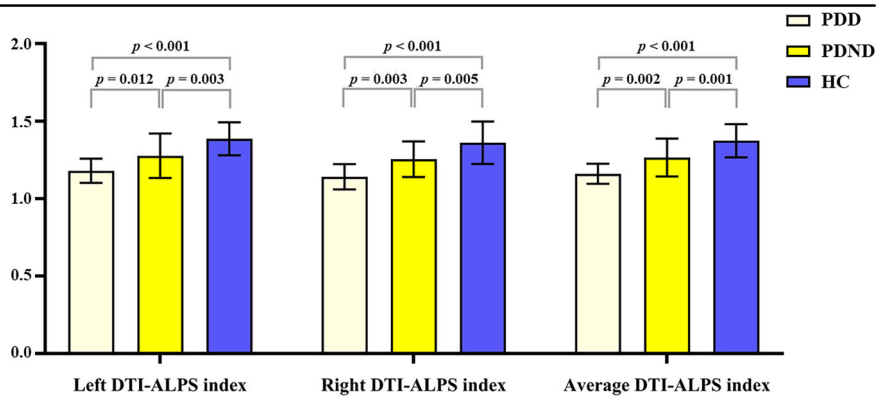

Fig. 1 | Comparison of DTI-ALPS indices across groups. The left, right and average DTI-ALPS indices in PDD, PDND and HC. DTI-ALPS diffusion tensor imaging analysis along the perivascular space, PD Parkinson's disease, PDD PD patients with depression, PDND PD patients with non-depression, HC healthy control.

Table 3 | Between-group differences among PDD, PDND, and HC groups in seed-based FC values

Region	Patients		HC	MNI coordinates			Cluster size	*F* value	*P* value
	PDD	PDND		X	Y	Z			
mPFC_R	0.043 ± 0.082	0.149 ± 0.122	−0.038 ± 0.127	8	54	40	107	17.049	0.000[a]
MTG_R	0.034 ± 0.113	0.129 ± 0.110	−0.051 ± 0.108	56	−38	6	136	16.296	0.000[a]
ITG_R	−0.061 ± 0.154	0.132 ± 0.144	0.026 ± 0.104	52	8	−40	41	12.288	0.000[a]

mPFC medial prefrontal cortex, *MTG* middle temporal gyrus, *ITG* inferior temporal gyrus, *R* right, *MNI* Montreal Neurological Institute, *PD* Parkinson's disease, *PDD* PD patients with depression, *PDND* PD patients with non-depression, *HC* healthy control.
[a]*p* values were obtained by one-way analysis of variance (ANOVA) test.

BNST-mPFC_R, BNST-MTG_R and BNST-ITG_R were significantly different among three groups, with the seed-based FC values of the BNST-mPFC_R, BNST-MTG_R and BNST-ITG_R being higher in PDND than in PDD, and the seed-based FC values of the BNST-mPFC_R and BNST-MTG_R being higher in PDD than in HC; (3) the top 70 meaningful features in the mPFC_R, MTG_R and ITG_R significantly contributed to the classifier's ability to discriminate PDD from PDND with high accuracy; (4) the seed-based FC values in the right ITG were positively correlated with the HAMD scores, the left DTI-ALPS index was negatively correlated with the HAMD scores and the seed-based FC values in the right mPFC. However, we found no correlation between the DTI-ALPS indices and HAMA, MMSE scores in PDD.

MRI scans after intrathecal or intravenous injection of contrast agents were the traditional method to measure glymphatic function, but patient's compliance was poor due to the invasive nature and concerns for the side effects of the contrast agents. According to the unique anatomical profile of the periventricular region in the basal ganglia, in which the perivascular space along the medullary blood vessels as the main drainage channel of the glymphatic system runs in a right-left orientation perpendicular to the ventricular wall, the projection fibers adjacent to the lateral ventricle and the association fibers run perpendicular to the perivascular space in a head-foot orientation and in an anterior-posterior orientation, respectively. Taoka proposed the DTI-ALPS index to examine the glymphatic activities at the level of the lateral ventricle body by calculating the diffusivities of association and projection fibers[16]. It is a non-invasive, robust, and accepted by most researchers as an indirect index for evaluating glymphatic function. A recent study confirmed a good correlation between the DTI-ALPS index and glymphatic function measured by conventional MRI[28].

Glymphatic dysfunction measured by DTI-ALPS was observed in neurodegenerative diseases, especially in PD[14,29–32]. Our findings were consistent with previous studies that demonstrated a decrease in glymphatic function, suggesting that glymphatic dysfunction was a potential cause or outcome of PD. In our study, the DTI-ALPS indices declined more in PDD than in PDND, speculating that depression as a superimposed symptom of PD further contributes to glymphatic dysfunction. One published study demonstrated the asynchronous impairment of glymphatic function in both hemispheres in PD, with the left hemisphere being more vulnerable[14]. However, the asynchrony was not observed in the present study, and we

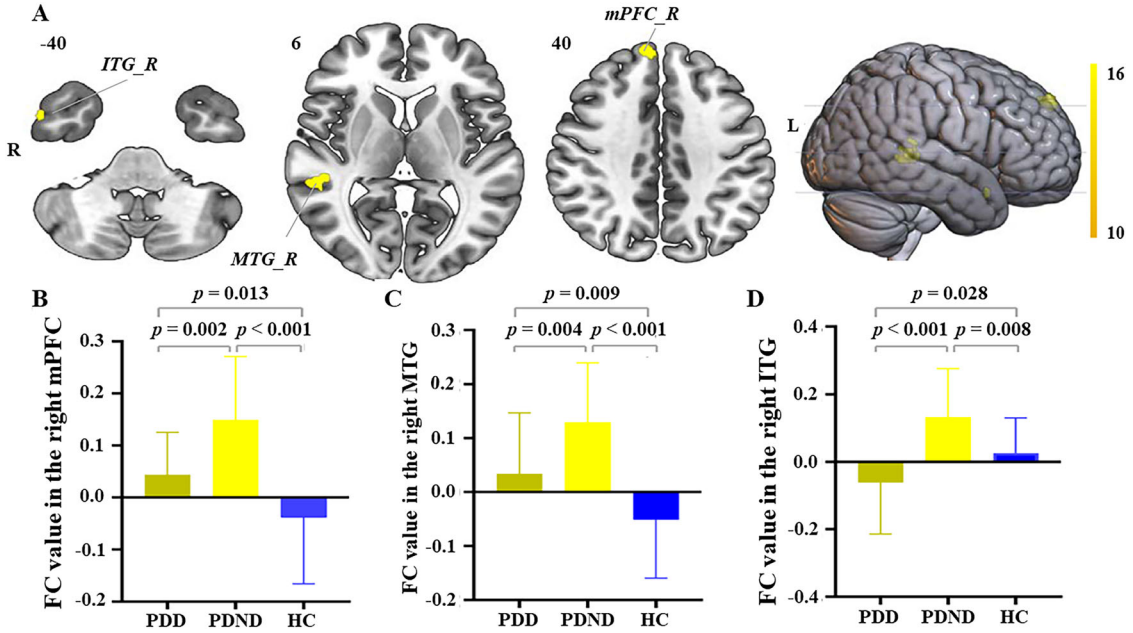

Fig. 2 | Seed-based functional connectivity differences in the right BNST region. **A** Brain regions and their coordinates showing between-group differences in seed-based FC values. **B–D** Bar plots of FC values between the right BNST and (**B**) medial prefrontal cortex (mPFC), (**C**) middle temporal gyrus (MTG), and (**D**) inferior temporal gyrus (ITG) in PDD, PDND, and HC groups. mPFC medial prefrontal cortex, MTG middle temporal gyrus, ITG inferior temporal gyrus, FC functional connectivity, PD Parkinson's disease, PDD PD patients with depression, PDND PD patients with non-depression, HC healthy control, L left, R right.

Table 4 | The weight of features to discriminate PDD from PDND

Weight	Region	MNI coordinates			Peak intensity	Cluster size
		X	Y	Z		
Negative weight	ITG_R	50	0	−42	−0.522	18
	MTG_R	58	−36	6	−0.490	22
	mPFC_R	6	56	38	−0.459	30

R right, *ITG* inferior temporal gyrus, *MTG* middle temporal gyrus, *mPFC* medial prefrontal cortex, *MNI* Montreal Neurological Institute, *PD* Parkinson's disease, *PDD* PD patients with depression, *PDND* PD patients with non-depression.

speculated that it should be acknowledged as a general pattern in glymphatic studies and needs to be confirmed by longitudinal studies. As a cerebrospinal fluid (CSF)-mediated pathway, the glymphatic system facilitates the fluid exchange and removal of metabolic waste in the brain[33–35]. Decreased expression of AQP4, an important component of the glymphatic system, increases the pathological deposition of α-synuclein, which promotes dopamine neuron loss. Cui et al.[36] demonstrated that the decreased expression of aquaporin (AQP4) in mice, an important component of the glymphatic system, increased the pathological deposition of α-synuclein and contributed to the loss of dopaminergic neurons. Several studies have shown that increased oxidative stress may impair the convective flow and CSF-to-interstitial fluid (ISF) turnover, and may act as a trigger for the degeneration process of dopaminergic neurons in PD[37–40]. The literature revealed that atherosclerosis and aging are risk factors for glymphatic dysfunction[29,30,41]. Therefore, we speculated that these risk factors and pathogenic pathways may cause damage to the glymphatic system.

Although glucocorticoids are adaptive in nature and prolonged exposure to their effects leads to severe metabolic, immune, and psychological dysfunction, glucocorticoid secretion is tightly regulated by the hypothalamic-pituitary-adrenal (HPA) axis[42]. Dysfunction in the basal forebrain that regulates the HPA axis, such as the hippocampus, amygdala, and medial prefrontal cortex (MPFC)[43,44], has implications for the etiology of stress-related conditions, including post-traumatic stress disorder (PTSD) and depression, which often manifest as abnormalities in the HPA axis[45,46]. The BNST is a highly specialized brain region containing numerous subregions and specific neurons, and a large amount of information from basal forebrain regions is integrated into the corresponding BNST subregions, which can either excite or inhibit HPA activity[21,47–50]. Studies have shown that patients with major depressive disorder (MDD) suffer from disturbed electrophysiological activity, particularly an excess of alpha-band oscillations in the BNST[51]. In animal models, electrical stimulation of the BNST has been shown to have antianxiety and antidepressant effects[42]. We infer that BSNT abnormalities might be related to the HPA axis activation in response to stress, and the decreased glucocorticoid levels may account for the reduced expression of depressive-like behaviors. However, this hypothesis warrants further investigation.

The BNST displays functional connectivity with the amygdala, medial prefrontal cortex (mPFC), caudate nucleus, thalamus, and hypothalamus, especially the mPFC[21]. Pizzagalli et al.[52] showed that the mPFC plays an important role in depression. We found that the enhanced FC connection between the right BNST and mPFC_R; the results from SVM also uncovered that the rich features embedded within the right mPFC can distinguish PDD from PDND; these results further confirmed and extended the previous findings. Based on the upstream afferent information that was integrated by the BNST and then projected to the corresponding downstream brain regions, we recognize that a possible mechanism of depression in PD is that the right BNST acts as a switching relay point.

In our study, there was a correlation between the left decreased DTI-ALPS index, right increased BNST-ITG FC values, and HAMD scores, suggesting that these indicators may serve as biomarkers to reflect the progression of affective symptoms in PDD. Moreover, the left DTI-ALPS indices were negatively correlated with the BNST-mPFC_R FC values and HAMD scores, indicating that the BNST-mPFC_R FC may mediate the impaired glymphatic function and depressive symptom in PD. This finding is consistent with that of Chen (2023), who used multiple approaches to reveal that the prelimbic mPFC to the anterior ventral bed nucleus of the stria terminalis (avBNST) circuit is a target for regulating depression[27].

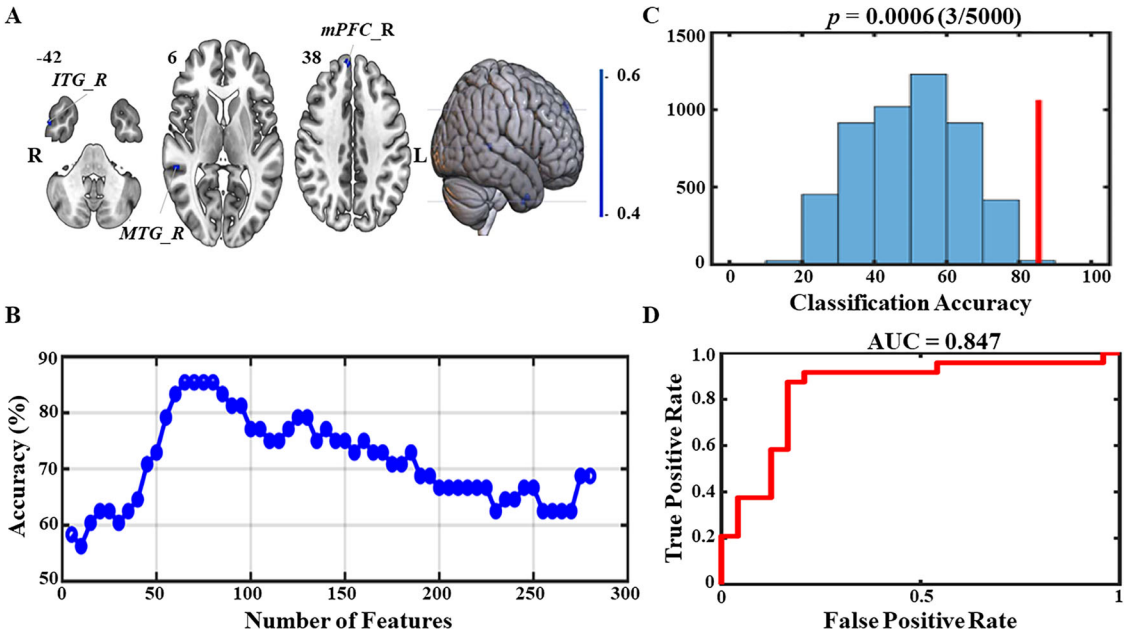

Fig. 3 | Feature selection and validation of the classification model. A Brain regions (right medial prefrontal cortex [mPFC_R], middle temporal gyrus [MTG_R], and inferior temporal gyrus [ITG_R]) showing significant between-group differences in seed-based functional connectivity values, selected as input features. **B** Model accuracy (y-axis) as a function of the number of features (x-axis). **C** Permutation test results (5000) showing the distribution of null accuracy (histogram) and observed accuracy (red vertical line). **D** The ROC curve of the binary classification model and its AUC value. mPFC medial prefrontal cortex, MTG middle temporal gyrus, ITG inferior temporal gyrus, L left, R right, ROC receiver operating characteristic, AUC area under curve.

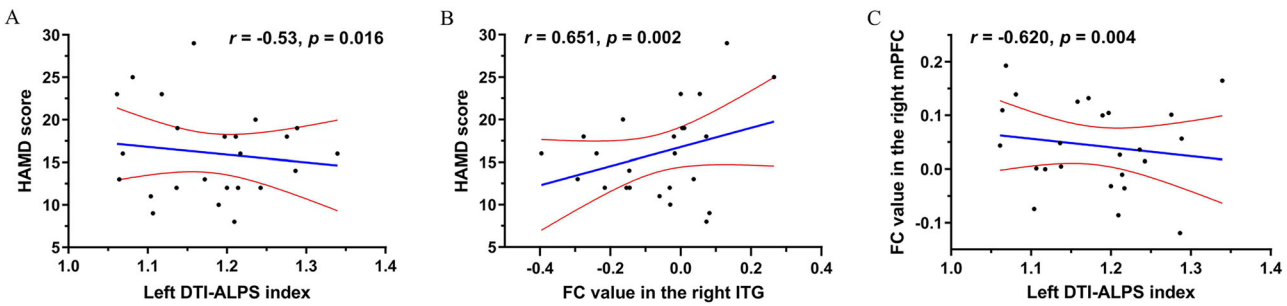

Fig. 4 | Correlations between DTI-ALPS indices, functional connectivity, and depression severity. A Scatter plot showing a negative correlation between the left DTI-ALPS index and HAMD scores. **B** Positive correlation between seed-based FC values in the right ITG and HAMD scores. **C** Negative association between the left DTI-ALPS index and FC values in the right mPFC. DTI-ALPS diffusion tensor imaging analysis along the perivascular space, HAMD Hamilton Depression Scale, FC functional connectivity, ITG inferior temporal gyrus, mPFC medial prefrontal cortex.

Our study has several limitations. First, we cannot yet determine the causal relationship between glymphatic function and PD because of the baseline data used for analysis. Therefore, longitudinal data with a larger sample size are needed in the future. Second, the DTI-ALPS index is an indirect measure of glymphatic function in the basal ganglia. Although a recent study confirmed the correlation between the DTI-ALPS index and glymphatic function measured by conventional MRI[28], the results associated with this non-invasive approach should still be interpreted with caution. Third, single-shell acquisition makes it challenging to estimate the intravoxel structure up to the desired resolution, and multi-shell acquisition (multiple b-values) will be essential for diffusion imaging in future research. Fourth, a key limitation of this study is that it did not account for the potential effects of Parkinsonian and antidepressant medications on functional connectivity and glymphatic function. Existing research has demonstrated that antidepressants can modulate functional connectivity between the default mode network (DMN) and the salience network (SN)[53], dopaminergic medications may enhance striato-cortical functional connectivity[54], and certain anesthetic agents can significantly impair glymphatic clearance efficiency[55]. Therefore, future studies should include detailed records of participants' medication use and analyze the specific effects of different medications on functional connectivity and glymphatic function. This will help to provide a more comprehensive understanding of the neurobiological mechanisms of these disorders and their treatments.

In conclusion, impaired glymphatic function and altered BNST-based FC are strongly associated with PD, and brain regions with differences in the BNST-mPFC_R, BNST-MTG_R, and BNST-ITG_R FC may serve as potential biomarkers for the classification of clinical subtypes of PD. These findings provide new insights into the pathogenesis of depression in PD.

Methods

Participants

This study was a case-control trial. The protocol was approved by the Ethics Committee of the Second Affiliated Hospital of Guangzhou University of Chinese Medicine. Before initiation of this inquiry, the aims and experimental procedures of this study were fully explained to all participants, and they gave their written informed consent, according to the guidelines of the Declaration of Helsinki. This study protocol was registered on the Chinese

Clinical Trial Registry (ChiCTR2000038411, September 22, 2020, https://www.chictr.org.cn/showproj.html?proj=56715).

We consecutively recruited participants from the Parkinson's Disease Clinic of the Second Affiliated Hospital of Guangzhou University of Chinese Medicine between April 2021 and March 2023. The diagnosis of PD was made by two experienced neurologists based on the United Kingdom PD Society Brain Bank. Inclusion criteria were as follows: (1) patients diagnosed with idiopathic PD[56]; (2) PD diagnosis of 1 to 3 according to the Hoehn and Yahr (H-Y) scale; (3) diagnosis over 2 years; (4) patients with asymmetric bradykinesia or asymmetric resting tremor, or both, including resting tremor, bradykinesia and rigidity; (5) patients being right-handed Han Chinese; (6) patients aged 40 to 75 years. Patients were excluded as follows: participants with (1) Parkinson's syndrome (i.e., vascular Parkinson's disease, encephalitis, or drug-induced syndromes); (2) Parkinson's superposition syndrome, (i.e., progressive supranuclear palsy, multiple system atrophy, or corticobasal degeneration); (3) any psychiatric disorders, (i.e., epilepsy, schizophrenia, bipolar disorder); (4) brain parenchymal lesions on MRI (i.e., brain tumors, stroke, brain trauma); (5) a history of antidepressant medication; (6) substance use disorders (i.e., alcohol, nicotine); (7) severe cognitive impairment (Mini-Mental State Examination, MMSE < 24); and (8) contraindications to MRI examinations (i.e., claustrophobia).

Depression was assessed by an experienced psychiatrist using the Diagnostic and Statistical Manual of Mental Disorders, Fifth Edition (DSM-5). Meanwhile, healthy individuals matched for sex, age, and education were recruited for controls by advertisements and word of mouth. In the end, 24 PD with depression, 24 PD without depression, and 25 HC were included in this study.

Clinical assessments

A neurologist blinded to the clinical information evaluated all patients who were required to discontinue anti-Parkinson's drugs for at least 12 h prior to clinical assessment. The Unified Parkinson's Disease Rating Scale (UPDRS) was used to assess the severity of PD. The scale is divided into three parts: the first section to assess mental activity, behavior, and emotional disorders; the second section to examine activities of daily living; and the third section to evaluate motor functionality. The Hoehn-Yahr (H-Y) scale was used to document the condition of PD patients. Neuropsychological measurements included the Hamilton Anxiety Scale (HAMA) and the Hamilton Depression Scale (HAMD-24) for assessing the psychological status; the Parkinson's Disease Sleepiness Scale, Second Edition (PDSS-2) for measuring sleep disorders[57]; and the MMSE for cognitive function during the on-stage of patients. PD was assigned into depressed and non-depressed patients based on HAMD scores (HAMD ≥ 8). In addition, comprehensive information on demographics, medical history, and L-dopa equivalent daily dose (LEDD) was also collected.

Magnetic resonance imaging acquisition

PD patients were requested to discontinue anti-Parkinson's drugs for at least 12 h prior to MRI scan to diminish any effects of drugs on brain activities. Imaging data were acquired on a 3.0 T Ingenia MRI scanner (Philips, Amsterdam, Netherlands) using a 32-channel head coil. All participants were instructed not to focus their minds on specific thoughts and to keep awake with eyes closed during scanning. Their heads were secured with foam padding to minimize head movement. MRI sequences included axial T2 fluid-attenuated inversion recovery (T2-FLAIR), diffusion tensor imaging (DTI), and blood oxygen level-dependent (BOLD), 3D-T1WI in this protocol, with T2-FLAIR used to exclude visible lesions. The detailed parameters were as follows: (1) BOLD, repetition time (TR) = 2000 ms, echo time (TE) = 30 ms, field of view (FOV) = 224 mm × 224 mm, matrix = 64 × 64, flip angle = 90°, slice thickness = 3.5 mm, interslice gap = 0.7 mm, 31 axial slices paralleled, and 240 time points; (2) DTI, TR = 3000 ms, TE = 88 ms, matrix = 112 × 112, FOV = 224 mm × 224 mm, voxel size = 2.0 × 2.0 × 2.0 mm^3, flip angle = 90°, 72 slices, slice thickness = 2 mm, 128 directions, and b = 1000 s/mm^2. Additionally, high-resolution 3D T1-weighted images were acquired for anatomical reference with the following parameters: TE = 4.5 ms, TR = 9.8 ms, FOV = 256 × 240 × 224 mm, matrix = 320 × 300, voxel size = 0.8 × 0.8 × 0.8 mm, flip angle = 9°, slice gap = 0 mm, slice thickness = 0.8 mm, number of slices = 280.

Diffusion tensor imaging data processing

Prior to preprocessing, all T2WI-FLAIR images were visually inspected by an experienced neuroradiologist to exclude participants with visible white matter hyperintensities (WMHs), lacunar infarcts, or other structural abnormalities. We used the FMRIB software library (FSL, http://www.fmrib.ox.ac.uk/fsl/) to perform the DTI-ALPS. The initial steps in processing each dataset included correction for motion, eddy currents, susceptibility artifacts, registration to standard space, and rotation of gradient tables. First, we used dcm2nii to convert the DTI images from the original data into 4D NIfTI format files. Then, the eddy_correct command was employed to correct the DTI images for both head motion and eddy currents to eliminate their effects. The fdt_rotate_bvecs command was utilized for the alignment of the corrected gradient direction table. Additionally, the skull was removed to yield a brain tissue mask. The FSL dtifit function was employed to generate tensor files in the three dimensions (x-axis, y-axis, and z-axis diffusivity) for each participant. Each tensor file was then aligned with its respective T1 image and normalized to MNI space using the SPM12 toolbox. The projection fibers next to the lateral ventricle ran along the z-axis direction, the association fibers ran along the y-axis direction, and the subcortical fibers ran along with the PVS in the x-axis direction (Fig. 5B). On the color-coded FA map, we placed a 5-mm diameter spherical region of interest (ROI) within the projection fibers, association fibers and subcortical fibers in bilateral hemispheres (Fig. 5A). Subsequently, diffusivities along various directions of these ROIs were extracted. Finally, the DTI-ALPS

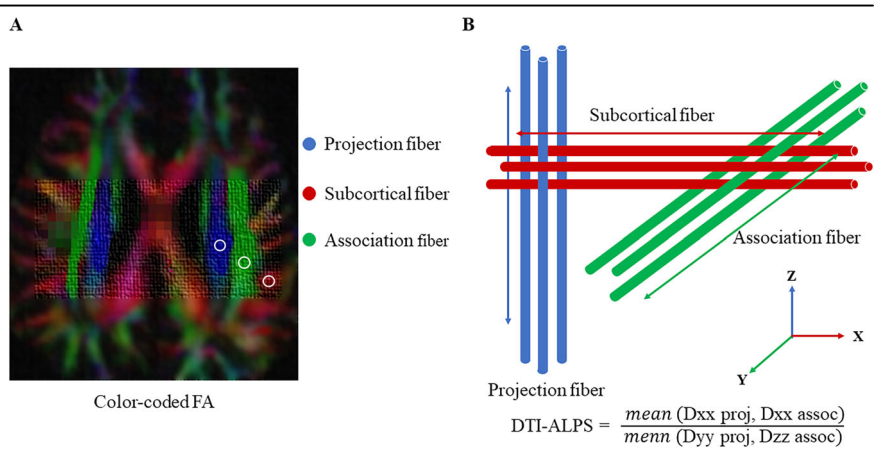

Fig. 5 | Methodology for calculating the DTI-ALPS index. A Color-coded fractional anisotropy (FA) map indicating fiber orientations: projection fibers (blue, z-axis), association fibers (green, y-axis), and subcortical fibers (red, x-axis). Three 5 × 5 mm^2 regions of interest (ROIs, white squares) were manually placed to measure diffusivity along each fiber type. **B** Schematic representation of the perivascular space (PVS) orientation relative to projection and association fibers. DTI diffusion tensor imaging analysis along the perivascular space, FA fractional anisotropy, PVS perivascular space, ROI region of interest.

index was calculated as [(Dxproj + Dxassoc)/(Dyproj + Dzassoc)] for each hemisphere[16]. The average values of the bilateral DTI-ALPS index were calculated as a measure of the glymphatic function. The DTI-ALPS index represents good diffusibility along the perivascular space, with higher values indicating better glymphatic function.

To ensure the reproducibility of DTI-ALPS index measurements, two independent raters performed the ROI placement and index calculation. Both raters were blinded to participants' clinical information.

Magnetic resonance imaging data preprocessing and seed-based functional connectivity

The resting-state fMRI data were analyzed based on statistical parametric mapping software (SPM12, http://www.fil.ion.ucl.ac.uk) for the MATLAB 2019a (https://www.mathworks.com) platform (MathWorks Inc., Nettick, MA, USA) using the Data Processing and Brain Imaging Analysis (DPABI) toolbox[58]. The preprocessing steps were as follows: (1) conversion of DICOM data to NIfTI format; (2) removal of the first 10 time points to reduce the effect of factors such as machine preheating on data quality; (3) slice time correction; (4) head motion correction with the Friston 24 parameter model, excluding subjects with head movements greater than 2° or greater than 2 mm in any direction, or volume-level mean framewise displacement (FD) more than 0.30 mm; (5) co-registration between the individual T1 structural volumes and the realigned functional volumes; (6) normalization into the Montreal Neurological Institute (MNI152) space through Diffeomorphic Anatomical Registration Through Exponentiated Lie Algebra (DARTEL)[59]; (7) spatial smoothing with a 6 mm full width at half maximum; (8) nuisance linear regression (white matter, cerebrospinal fluid, and Friston 24 head motion); and (9) linear trend removal and temporal bandpass (0. 01–0.1 Hz) filtering.

Based on the lateralization of emotional processing, the clinical lateralization of PD symptoms, and considerations of multiple comparison correction and statistical power, this study adopted an exploratory approach to select the right BNST as ROI[60–64].

We identified the BNST seed using a probabilistic atlas based on a manual BNST segmentation method developed by Torrisi and his colleagues[65], which has been widely used in previous studies[66–68]. Then, we calculated the Pearson's correlation coefficients between the ROI and the whole brain in a voxel-wise and obtained the FC values. After Fisher's Z-normalization, the r-values were converted to z-values for statistical analysis.

Support vector machine analysis

The core idea of SVM is to find a hyperplane with maximum marginal separation in high-dimensional space, which makes the support vector as far away from the nearest data points as possible. The classification analysis was performed using the LIBSVM toolbox (http://www.csie.ntu.edu.tw/~cjlin/libsvm/). The classification process consists of two steps: training and testing. First, we constructed a class vector consisting of "+1" (PDD) or "−1" (PDND). Then, using the seed-based FC values of the between-group differences as input, a classifier was built by the leave-one-out cross-validation (LOOCV) strategy, and the accuracy, sensitivity, and specificity were obtained. To assess the robustness of the model, a permutation test was also performed (N = 5000), with the significance threshold set at $p < 0.05$ (two-tailed). Finally, the area under the receiver operating curve (AUC) was calculated to examine the predictive performance of the established model.

During feature selection, the F-score algorithm was employed to rank the importance of each FC feature. The F-score quantifies a feature's discriminative power for classification by calculating the ratio of inter-group differences to intra-group variance. F-score values were calculated for all candidate features and ranked in descending order. The top 70 features (corresponding to the number of features at the accuracy peak in Fig. 3B) were selected for final classification. These features were from ROIs that showed significant inter-group differences, including the right inferior temporal gyrus (ITG_R), right middle temporal gyrus (MTG_R), and right medial prefrontal cortex (mPFC_R) (see Table 4).

Statistical analysis

Statistical analyses were conducted using SPSS (version 22.0; IBM, Armonk, NY, USA). First, we performed a descriptive analysis of demographic and clinical scale data. Continuous variables are described as mean ± standard deviation (SD), while categorical variables are shown as frequencies and percentages. The Kolmogorov-Smirnov test and the Shapiro-Wilk test were used to assess the normality and homogeneity of each group of variables.

For demographic and clinical data (i.e., age, education, HAMA, HAMD, MADRS, and MMSE), the Kruskal-Wallis test was used for between-group differences, and the Chi-square ($\chi 2$) test was used for categorical variables (i.e., gender). To adjust for the risk of type I error due to multiple comparisons, Bonferroni correction was used.

Based on the previous results of the Kolmogorov–Smirnov test and Shapiro-Wilk test, we used Kruskal-Wallis and one-way analysis of variance (ANOVA) test to detect the between-group differences in DTI-ALPS indices and seed-based FC values, respectively. Then, post-hoc *t*-tests were performed to identify the pairwise group differences with Bonferroni. Meanwhile, according to the results of the Kolmogorov-Smirnov test, Mann–Whitney test was used to detect the between-group differences of the Unified Parkinson's Disease Rating Scale (UPDRS) between PDD and PDND groups.

To explore the relationships between the DTI-ALPS indices (right, left, and average) and the clinical scale scores (i.e., HAMD, HAMA, and MMSE) and seed-based FC values, Pearson's correlation analyses were performed, adjusting for gender, age, education, and MMSE as covariates. All p values < 0.05 were considered statistically significant.

Data availability

Data will be made available on request.

Received: 21 July 2024; Accepted: 24 April 2025;
Published online: 16 May 2025

References

1. GBD 2016 Neurology Collaborators Global, regional, and national burden of neurological disorders, 1990–2016: a systematic analysis for the Global Burden of Disease Study 2016. *Lancet Neurol.* **18**, 459–480 (2019).
2. Ben-Shlomo, Y. et al. The epidemiology of Parkinson's disease. *Lancet* **403**, 283–292 (2024).
3. Pringsheim, T., Jette, N., Frolkis, A. & Steeves, T. D. The prevalence of Parkinson's disease: a systematic review and meta-analysis. *Mov. Disord.* **29**, 1583–1590 (2014).
4. Kim, B. S., Jang, T., Yoo, S. E., Lee, J. M. & Kim, E. Fas-associated factor 1 induces the accumulation of α-synuclein through autophagic suppression in dopaminergic neurons. *FASEB J.* **35**, e21363 (2021).
5. Dada, S. T. et al. Pharmacological inhibition of α-synuclein aggregation within liquid condensates. *Nat. Commun.* **15**, 3835 (2024).
6. Pan, L. et al. Tau accelerates α-synuclein aggregation and spreading in Parkinson's disease. *Brain* **145**, 3454–3471 (2022).
7. Lohela, T. J., Lilius, T. O. & Nedergaard, M. The glymphatic system: implications for drugs for central nervous system diseases. *Nat. Rev. Drug Discov.* **21**, 763–779 (2022).
8. Lee, S. et al. Contrast-enhanced MRI T1 mapping for quantitative evaluation of putative dynamic glymphatic activity in the human brain in sleep-wake states. *Radiology* **300**, 661–668 (2021).
9. Pavan, C. et al. DNase treatment prevents cerebrospinal fluid block in early experimental pneumococcal meningitis. *Ann. Neurol.* **90**, 653–669 (2021).
10. Cai, X. et al. Imaging the effect of the circadian light-dark cycle on the glymphatic system in awake rats. *Proc. Natl. Acad. Sci. USA* **117**, 668–676 (2020).
11. Bae, Y. J. et al. Altered brain glymphatic flow at diffusion-tensor mri in rapid eye movement sleep behavior disorder. *Radiology* **307**, e221848 (2023).

12. Yang, D. X. et al. Associations of MRI-derived glymphatic system impairment with global white matter damage and cognitive impairment in mild traumatic brain injury: a DTI-ALPS study. *J. Magn. Reson Imaging* **59**, 639–647 (2024).
13. Margoni, M. et al. Cognitive impairment is related to glymphatic system dysfunction in pediatric multiple sclerosis. *Ann. Neurol.* **95**, 1080–1092 (2024).
14. Shen, T. et al. Diffusion along perivascular spaces as marker for impairment of glymphatic system in Parkinson's disease. *NPJ Parkinsons Dis.* **8**, 174 (2022).
15. Xu, K. et al. Evaluation of glymphatic system activity by diffusion tensor image analysis along the perivascular space in presbycusis. *CNS Neurosci. Ther.* **30**, e14458 (2024).
16. Taoka, T. et al. Evaluation of glymphatic system activity with the diffusion MR technique: diffusion tensor image analysis along the perivascular space (DTI-ALPS) in Alzheimer's disease cases. *Jpn J. Radio.* **35**, 172–178 (2017).
17. Khan, M. A., Quadri, S. A. & Tohid, H. A comprehensive overview of the neuropsychiatry of Parkinson's disease: a review. *Bull. Menninger Clin.* **81**, 53–105 (2017).
18. Schrag, A. & Taddei, R. N. Depression and anxiety in Parkinson's disease. *Int Rev. Neurobiol.* **133**, 623–655 (2017).
19. Pontone, G. M. et al. The longitudinal impact of depression on disability in Parkinson disease. *Int J. Geriatr. Psychiatry* **31**, 458–465 (2016).
20. Oler, J. A. et al. Evidence for coordinated functional activity within the extended amygdala of non-human and human primates. *Neuroimage* **61**, 1059–1066 (2012).
21. Lebow, M. A. & Chen, A. Overshadowed by the amygdala: the bed nucleus of the stria terminalis emerges as key to psychiatric disorders. *Mol. Psychiatry* **21**, 450–463 (2016).
22. Vranjkovic, O., Pina, M., Kash, T. L. & Winder, D. G. The bed nucleus of the stria terminalis in drug-associated behavior and affect: a circuit-based perspective. *Neuropharmacology* **122**, 100–106 (2017).
23. Ch'ng, S., Fu, J., Brown, R. M., McDougall, S. J. & Lawrence, A. J. The intersection of stress and reward: BNST modulation of aversive and appetitive states. *Prog. Neuropsychopharmacol. Biol. Psychiatry* **87**, 108–125 (2018).
24. Fitzgerald, P. B. et al. A pilot study of bed nucleus of the stria terminalis deep brain stimulation in treatment-resistant depression. *Brain Stimul.* **11**, 921–928 (2018).
25. Nagai, M. M., Gomes, F. V., Crestani, C. C., Resstel, L. B. & Joca, S. R. Noradrenergic neurotransmission within the bed nucleus of the stria terminalis modulates the retention of immobility in the rat forced swimming test. *Behav. Pharmacol.* **24**, 214–221 (2013).
26. Wang, T. et al. Parameter-based analysis of clinical efficacy of combined bed nucleus of the stria terminalis-nucleus accumbens deep brain stimulation for treatment-resistant depression. *J. Neurosurg.* **140**, 1630–1640 (2024).
27. Chen, J. Y. et al. The PrLGlu→avBNSTGABA circuit rapidly modulates depression-like behaviors in male mice. *iScience* **26**, 107878 (2023).
28. Zhang, W. et al. Glymphatic clearance function in patients with cerebral small vessel disease. *Neuroimage* **238**, 118257 (2021).
29. Meng, J. C. et al. Correlation of glymphatic system abnormalities with Parkinson's disease progression: a clinical study based on non-invasive fMRI. *J. Neurol.* **271**, 457–471 (2024).
30. Cai, X. et al. Diffusion along perivascular spaces provides evidence interlinking compromised glymphatic function with aging in Parkinson's disease. *CNS Neurosci. Ther.* **29**, 111–121 (2023).
31. Chen, B. et al. Functional connectome automatically differentiates multiple system atrophy (parkinsonian type) from idiopathic Parkinson's disease at early stages. *Hum. Brain Mapp.* **44**, 2176–2190 (2023).
32. Qin, Y. et al. Neuroimaging uncovers distinct relationships of glymphatic dysfunction and motor symptoms in Parkinson's disease. *J. Neurol.* **270**, 2649–2658 (2023).
33. Iliff, J. J. et al. A paravascular pathway facilitates CSF flow through the brain parenchyma and the clearance of interstitial solutes, including amyloid β. *Sci. Transl. Med.* **4**, 147ra111 (2012).
34. Nedergaard, M. & Goldman, S. A. Glymphatic failure as a final common pathway to dementia. *Science* **370**, 50–56 (2020).
35. Rasmussen, M. K., Mestre, H. & Nedergaard, M. The glymphatic pathway in neurological disorders. *Lancet Neurol.* **17**, 1016–1024 (2018).
36. Cui, H. et al. Decreased AQP4 expression aggravates α-synuclein pathology in Parkinson's disease mice, possibly via impaired glymphatic clearance. *J. Mol. Neurosci.* **71**, 2500–2513 (2021).
37. Chen, H. L. et al. Associations among cognitive functions, plasma DNA, and diffusion tensor image along the perivascular space (DTI-ALPS) in patients with parkinson's disease. *Oxid. Med. Cell Longev.* **2021**, 4034509 (2021).
38. Erickson, M. A. et al. Lipopolysaccharide impairs amyloid β efflux from brain: altered vascular sequestration, cerebrospinal fluid reabsorption, peripheral clearance and transporter function at the blood-brain barrier. *J. Neuroinflam.* **9**, 150 (2012).
39. Trist, B. G., Hare, D. J. & Double, K. L. Oxidative stress in the aging substantia nigra and the etiology of Parkinson's disease. *Aging Cell* **18**, e13031 (2019).
40. Hwang, O. Role of oxidative stress in Parkinson's disease. *Exp. Neurobiol.* **22**, 11–17 (2013).
41. Da Mesquita, S. et al. Aging-associated deficit in CCR7 is linked to worsened glymphatic function, cognition, neuroinflammation, and β-amyloid pathology. *Sci. Adv.* **7**, eabe4601 (2021).
42. Crestani, C. C., Alves, F. H., Correa, F. M., Guimarães, F. S. & Joca, S. R. Acute reversible inactivation of the bed nucleus of stria terminalis induces antidepressant-like effect in the rat forced swimming test. *Behav. Brain Funct.* **6**, 30 (2010).
43. Pittenger, C. & Duman, R. S. Stress, depression, and neuroplasticity: a convergence of mechanisms. *Neuropsychopharmacology* **33**, 88–109 (2008).
44. Koenigs, M. & Grafman, J. The functional neuroanatomy of depression: distinct roles for ventromedial and dorsolateral prefrontal cortex. *Behav. Brain Res.* **201**, 239–243 (2009).
45. de Kloet, C. S. et al. Assessment of HPA-axis function in posttraumatic stress disorder: pharmacological and non-pharmacological challenge tests, a review. *J. Psychiatr. Res.* **40**, 550–567 (2006).
46. Pariante, C. M. & Lightman, S. L. The HPA axis in major depression: classical theories and new developments. *Trends Neurosci.* **31**, 464–468 (2008).
47. Stephens, S. B. Z. et al. Estradiol-dependent and -independent stimulation of kiss1 expression in the amygdala, BNST, and lateral septum of mice. *Endocrinology* **159**, 3389–3402 (2018).
48. Bota, M., Sporns, O. & Swanson, L. W. Neuroinformatics analysis of molecular expression patterns and neuron populations in gray matter regions: the rat BST as a rich exemplar. *Brain Res.* **1450**, 174–193 (2012).
49. Jennings, J. H., Rizzi, G., Stamatakis, A. M., Ung, R. L. & Stuber, G. D. The inhibitory circuit architecture of the lateral hypothalamus orchestrates feeding. *Science* **341**, 1517–1521 (2013).
50. Hao, S. et al. The lateral hypothalamic and BNST GABAergic projections to the anterior ventrolateral periaqueductal gray regulate feeding. *Cell Rep.* **28**, 616–624.e5 (2019).
51. Neumann, W. J. et al. Different patterns of local field potentials from limbic DBS targets in patients with major depressive and obsessive compulsive disorder. *Mol. Psychiatry* **19**, 1186–1192 (2014).
52. Pizzagalli, D. A. & Roberts, A. C. Prefrontal cortex and depression. *Neuropsychopharmacology* **47**, 225–246 (2022).
53. Cui, J. et al. Effects of escitalopram therapy on resting-state functional connectivity of subsystems of the default mode network in unmedicated patients with major depressive disorder. *Transl. Psychiatry* **11**, 634 (2021).

54. Kishore, A., Joseph, T., Velayudhan, B., Popa, T. & Meunier, S. Early, severe and bilateral loss of LTP and LTD-like plasticity in motor cortex (M1) in de novo Parkinson's disease. *Clin. Neurophysiol.* **123**, 822–828 (2012).
55. Gakuba, C. et al. Generam. *Theranostics* **8**, 710–722 (2018).
56. Postuma, R. B. et al. MDS clinical diagnostic criteria for Parkinson's disease. *Mov. Disord.* **30**, 1591–1601 (2015).
57. Trenkwalder, C. et al. Parkinson's disease sleep scale–validation of the revised version PDSS-2. *Mov. Disord.* **26**, 644–652 (2011).
58. Yan, C. G., Craddock, R. C., Zuo, X. N., Zang, Y. F. & Milham, M. P. Standardizing the intrinsic brain: towards robust measurement of inter-individual variation in 1000 functional connectomes. *Neuroimage* **80**, 246–262 (2013).
59. Ashburner, J. A fast diffeomorphic image registration algorithm. *Neuroimage* **38**, 95–113 (2007).
60. Baas, D., Aleman, A. & Kahn, R. S. Lateralization of amygdala activation: a systematic review of functional neuroimaging studies. *Brain Res. Rev.* **45**, 96–103 (2004).
61. Mayberg, H. S. Modulating dysfunctional limbic-cortical circuits in depression: towards development of brain-based algorithms for diagnosis and optimised treatment. *Br. Med. Bull.* **65**, 193–207 (2003).
62. Tomlinson, C. L. et al. Systematic review of levodopa dose equivalency reporting in Parkinson's disease. *Mov. Disord.* **25**, 2649–2653 (2010).
63. Hanganu, A. et al. Depressive symptoms in Parkinson's disease correlate with cortical atrophy over time. *Brain Cogn.* **111**, 127–133 (2017).
64. Poldrack, Russell A., Jeanette A. Mumford, and Thomas E. Nichols. *Handbook of Functional MRI Data Analysis*. (Cambridge University Press, 2024).
65. Torrisi, S. et al. Resting state connectivity of the bed nucleus of the stria terminalis at ultra-high field. *Hum. Brain Mapp.* **36**, 4076–4088 (2015).
66. Pang, M. et al. Resting-state causal connectivity of the bed nucleus of the stria terminalis in panic disorder. *Brain Imaging Behav.* **15**, 25–35 (2021).
67. Siminski, N. et al. BNST and amygdala activation to threat: effects of temporal predictability and threat mode. *Behav. Brain Res.* **396**, 112883 (2021).
68. Siminski, N. et al. Centromedial amygdala is more relevant for phobic confrontation relative to the bed nucleus of stria terminalis in patients with spider phobia. *J. Psychiatr. Res.* **143**, 268–275 (2021).

Acknowledgements

This work had support from supported by the Guangzhou Science and Technology Basic Research Project (202102010260), Project of Administration of Guangdong Provincial Traditional Chinese Medicine (20241130), Hubei Provincial Natural Science Foundation (2025AFD536) and Scientific Research Project of Traditional Chinese Medicine of Hubei Provincial Health Commission (ZY2025L284).

Author contributions

X.D.: conceptualization, methodology, software, investigation, formal analysis, writing-original draft; Y.Z.: methodology, software, formal analysis; C.F.: data curation, investigation; Z.G.: data curation, supervision; X.H.: data curation, validation; Z.Y.: software, visualization; C.Z.: resources, visualization; L.G.: validation, writing-review-editing; B.L.: conceptualization, funding acquisition, resources, project administration, supervision, writing-review-editing.

Competing interests

The authors declare no competing interests.

Additional information

Correspondence and requests for materials should be addressed to Bo Liu.